III. MICROWAVE SPECTROSCOPY*

Prof. M. W. P. Strandberg
Prof. R. L. Kyhl
Dr. D. H. Douglass, Jr.
J. M. Andrews, Jr.
W. J. C. Grant
R. Huibonhoa
J. G. Ingersoll
P. F. Kellen
J. D. Kierstead
J. W. Mayo
W. J. Schwabe
J. R. Shane
N. Tepley
S. H. Wemple

A. LINE SHAPES OF PARAMAGNETIC CHROMIUM RESONANCE IN RUBY

In a previous report,[1] we presented a general expression for the paramagnetic resonance line shape of magnetically dilute crystals, with particular reference to Cr^{+++} in ruby. The line shape was derived from magnetic dipole interactions. The detailed lattice structure, the possibility of clustering, and the effect of strong exchange forces over some arbitrary radius were taken into consideration. We quote the principal result:

$$I(\omega) = \int_{-\infty}^{\infty} e^{-i\omega\rho} e^{-nV'} \tag{1}$$

$$V' = \frac{1}{\Sigma g_j}\left[\sum_k g_k \sum_{r_i<r_1}\left(1-e^{i\rho\omega(\vec{r}_i, s_k)}\right)\right.$$

$$\left. + \sum_j g_j \sum_{r_1<r_i<r_o}\left(1-e^{i\rho\omega(\vec{r}_i, s_j)}\right) + \frac{2\pi}{3v}\frac{\Sigma g_j V_j}{\Sigma g_j}\right] \tag{2}$$

The symbols are explained in the previous report.[1] The quantities V_j were given in various series expansions. For the sake of compactness we now rewrite (2), with slight notational changes, as follows:

$$V' = \frac{\Sigma_a g_a\left(1-e^{i\rho\omega_a}\right)}{\Sigma g_j} + V_c(\rho). \tag{3}$$

The transform of $e^{-nV_c(\rho)}$ has been computed numerically for various values of the concentration n and inner cutoff radius r_o, and will be discussed in more detail below. The transform of the lattice sum (indexed on a) is obtained, to first order in n, as follows:

---

*This work was supported in part by the U.S. Army Signal Corps under Contract DA36-039-sc-87376; and in part by Purchase Order DDL B-00337 with Lincoln Laboratory, a center for research operated by Massachusetts Institute of Technology with the joint support of the U.S. Army, Navy, and Air Force under Air Force Contract AF19(604)-7400.

$$\int_{-\infty}^{\infty} d\rho\, e^{-i\omega\rho} \left\{ \exp\left[\frac{-n \sum_a g_a \left(1 - e^{i\rho\omega_a}\right)}{\sum_j g_j} \right] \right\}$$

$$\approx \exp\left(\frac{-n \sum_a g_a}{\sum_j g_j} \right) \int_{-\infty}^{\infty} d\rho\, e^{-i\omega\rho} \left[1 + n \frac{\sum_a g_a e^{i\rho\omega_a}}{\sum_j g_j} \right]$$

$$= \exp\left(-n \frac{\sum_a g_a}{\sum_j g_j} \right) \left[\delta(\omega) + \frac{n}{\sum_j g_j} \sum_a g_a \delta(\omega - \omega_a) \right]. \qquad (4)$$

Here, δ represents the delta function.

Since $V_c(\rho)$ and the lattice sum appear essentially as products in the ρ domain, their joint contribution in the ω domain is obtained by convolution. In this sense, expression (4) embodies the satellite spectrum and provides a simple prescription for adding it to the main line. The possibility of clustering can be taken into account at this point by varying n in (4).

Interactions other than Cr-Cr dipole broadening can be assimilated into the theory. In general, the joint effect of any number of statistically independent interactions is obtained by convoluting the separate effects.[2] Interactions with neighboring aluminum nuclei, for example, evidently fulfill the independence criterion for small Cr concentrations.

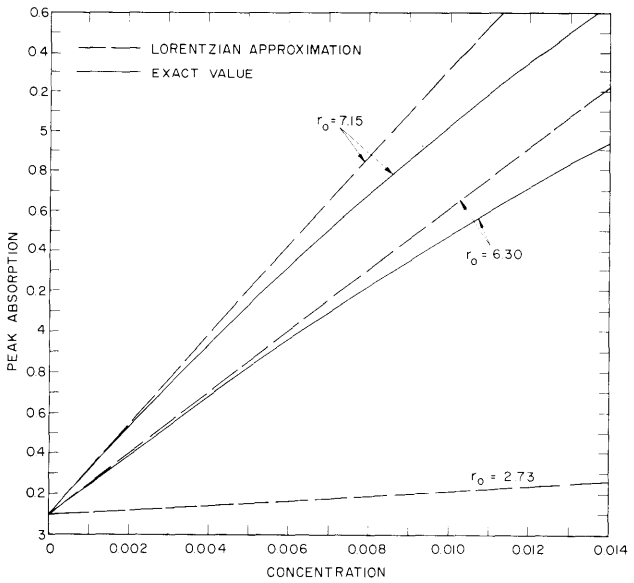

Fig. III-1. Peak absorption vs concentration for $\left(\frac{1}{2}, -\frac{1}{2}\right)$ transition (continuous dipole distribution).

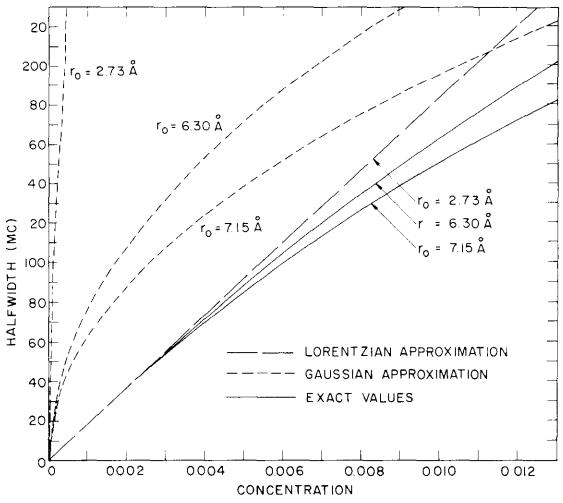

Fig. III-2. Halfwidth vs concentration for $\left(\frac{1}{2}, -\frac{1}{2}\right)$ transition (continuous dipole distribution).

In practice it has proved convenient to perform the numerical computations in the following sequence: (a) inversion of $\exp[-nV_c(\rho)]$, (b) convolution with a Gaussian to include non Cr-Cr interactions, and (c) convolution with the δ-functions of (4) to include the contribution of the near neighbors. We shall discuss these calculations in this order.

We calculated the line shape resulting from a continuous dipole distribution over a range of concentrations, 0.01 per cent $\leq n \leq$ 1.1 per cent, and over a range of cutoff radii, 2.73 Å $\leq r_o \leq$ 7.15 Å. The range of r_o goes from the nearest neighbor shell to the 16^{th} neighbor shell, which is a safe maximum for any resonable possibility of appreciable exchange forces. We stated in the previous report[1] that the leading terms in the expansions for $V_c(\rho)$ indicate a line shape that is Lorentzian in the center and Gaussian in the wings. Similarly, one can see that the line shape must become Lorentzian for small n and small r_o, and Gaussian for large n and large r_o.

In the Lorentzian limit,

$$\text{Halfwidth} = c_1 n \tag{5}$$

$$\text{Peak intensity} = c_2 + c_3 r_o^3 n. \tag{6}$$

In the Gaussian limit,

$$\text{Halfwidth} = c_4 r_o^{-3/2} n^{1/2} \tag{7}$$

$$\text{Peak intensity} = c_5 r_o^{3/2} n^{1/2}. \tag{8}$$

Here, c_1-c_5 are constants that depend on the detailed crystal structure and on the energy

levels of the particular ions in question. By halfwidth we mean the distance from the peak value to one-half the peak value. By concentration we mean the ratio of the number of Cr atoms to the total number of cations.

In Figs. III-1 and III-2 we show the dependence of intensity and halfwidth on concentration, r_o being constant, for the $\left(\frac{1}{2}, -\frac{1}{2}\right)$ transition in ruby. In Figs. III-3 and III-4 we show the same relations (for r_o = 7.15 Å only) for the $\left(\frac{3}{2}, \frac{1}{2}\right)$ transition. In Fig. III-5, we show the dependence of the halfwidth on r_o, with n constant, for the $\left(\frac{1}{2}, -\frac{1}{2}\right)$ transition. The line shapes are obviously close to being Lorentzian. Indeed, in Figs. III-1 and III-2, for r_o = 2.73 Å (the nearest neighbor distance), the exact calculated intensities and halfwidths cannot be distinguished, on the scale of our graph, from the Lorentzian limit. We note that in the Gaussian limit we set the halfwidth proportional to the square root of the second moment (with a proportionality factor of 1.175). Clearly, in dilute crystals, the Cr-Cr dipole interaction gives rise to line shapes of which neither the magnitudes nor the parametric dependences are related to the second moment in any simple fashion.

The second step in our computation takes into account interactions that are independent of Cr-Cr broadening. The contribution of such interactions can be isolated experimentally as the residual line shape in the limit of vanishing Cr concentration. This residual line turns out to be a Gaussian of halfwidth 17.75 mc. We shall discuss the origin of this line shape in Appendix A. We point out that 18 mc is the dipolar width at

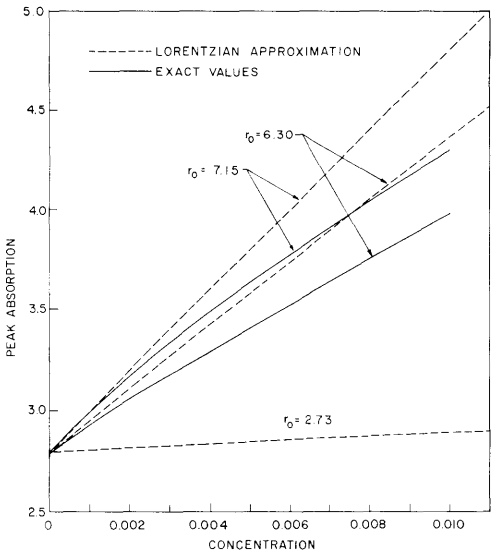

Fig. III-3. Peak absorption vs concentration for $\left(\frac{3}{2}, \frac{1}{2}\right)$ transition (continuous dipole distribution).

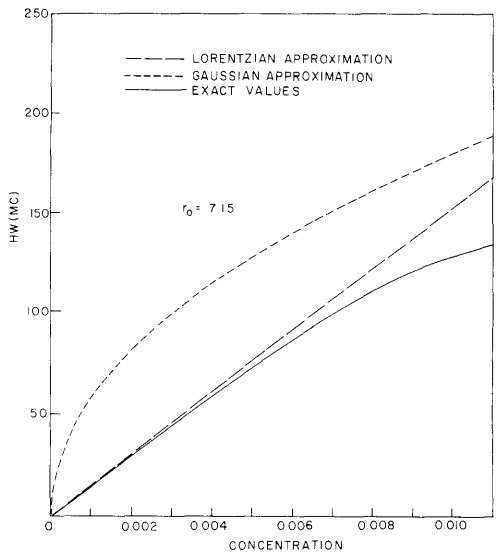

Fig. III-4. Halfwidth vs concentration for $\left(\frac{3}{2}, \frac{1}{2}\right)$ transition (continuous dipole distribution).

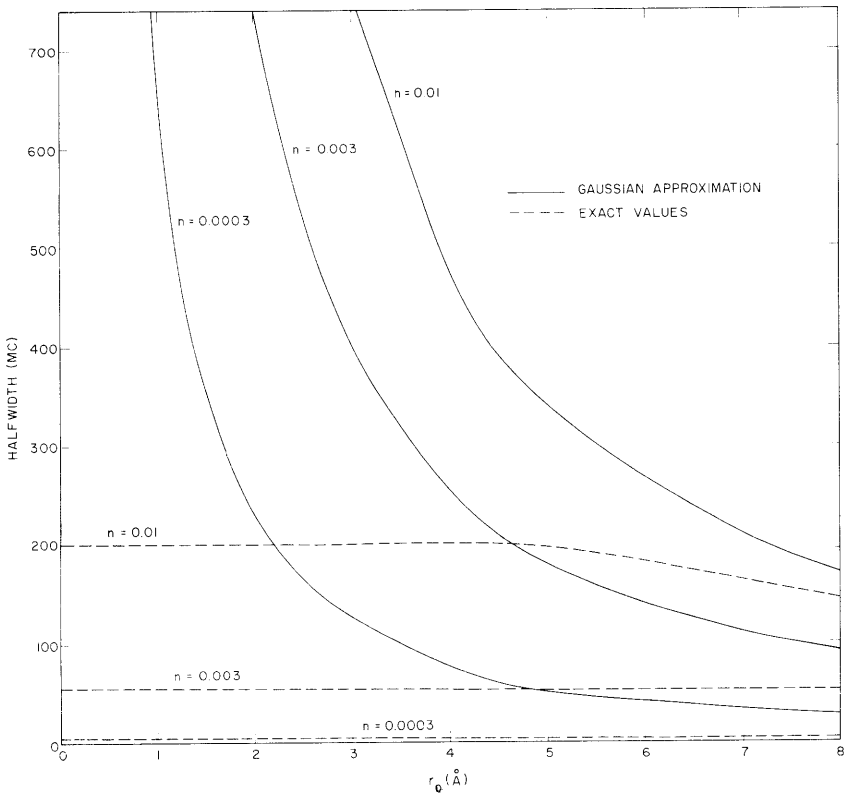

Fig. III-5. Halfwidth vs r_o for $\left(\frac{1}{2}, -\frac{1}{2}\right)$ transition (continuous dipole distribution).

~0.1 per cent concentration, almost independently of r_o. (See Fig. III-2.) This means that Cr self-broadening makes a very small contribution to the total line in "pink" ruby, accounts for roughly one-half the width in "standard" ruby, and becomes predominant only in "dark" ruby. Consequently, relations (5) and (6) do not apply to actually observed lines. Instead, for concentrations of ~0.01 per cent, one expects

$$\text{Halfwidth} \approx \text{constant} \approx 18 \text{ mc} \tag{9}$$

$$\text{Intensity} \propto n. \tag{10}$$

In Figs. III-6, III-7, and III-8 we display the pure Cr dipolar line (calculated for r_o = 7.15 Å), together with the convolution of this line with the 17.75-mc Gaussian, for concentrations of 0.02, 0.2, and 1.1 per cent. Only the highest concentration, for which the two line shapes almost coincide, does the Gaussian make a minor contribution.

In Figs. III-6 and III-8 we also show the result of including the lattice sum, which is the third step in our computation. We have assumed here a concentration of near neighbors which is consistent with a random distribution. One can see that the contribution of the near neighbors is negligible for the 0.02 per cent crystal (the dotted line almost coincides with the solid line), but is quite substantial for the 1.1 per cent crystal. The relative

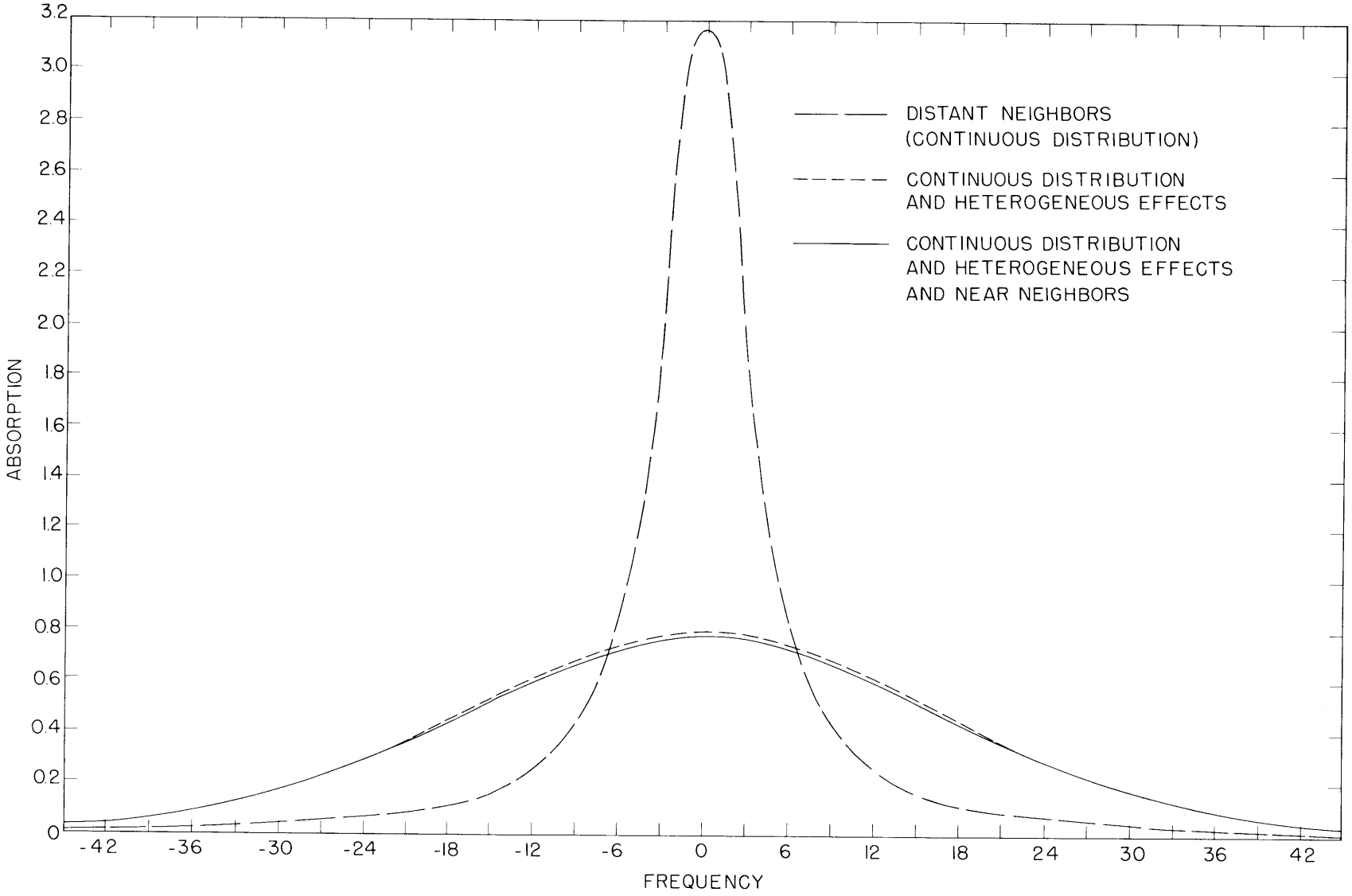

Fig. III-6. Contribution of various effects to the absorption (concentration, 0.02 per cent).

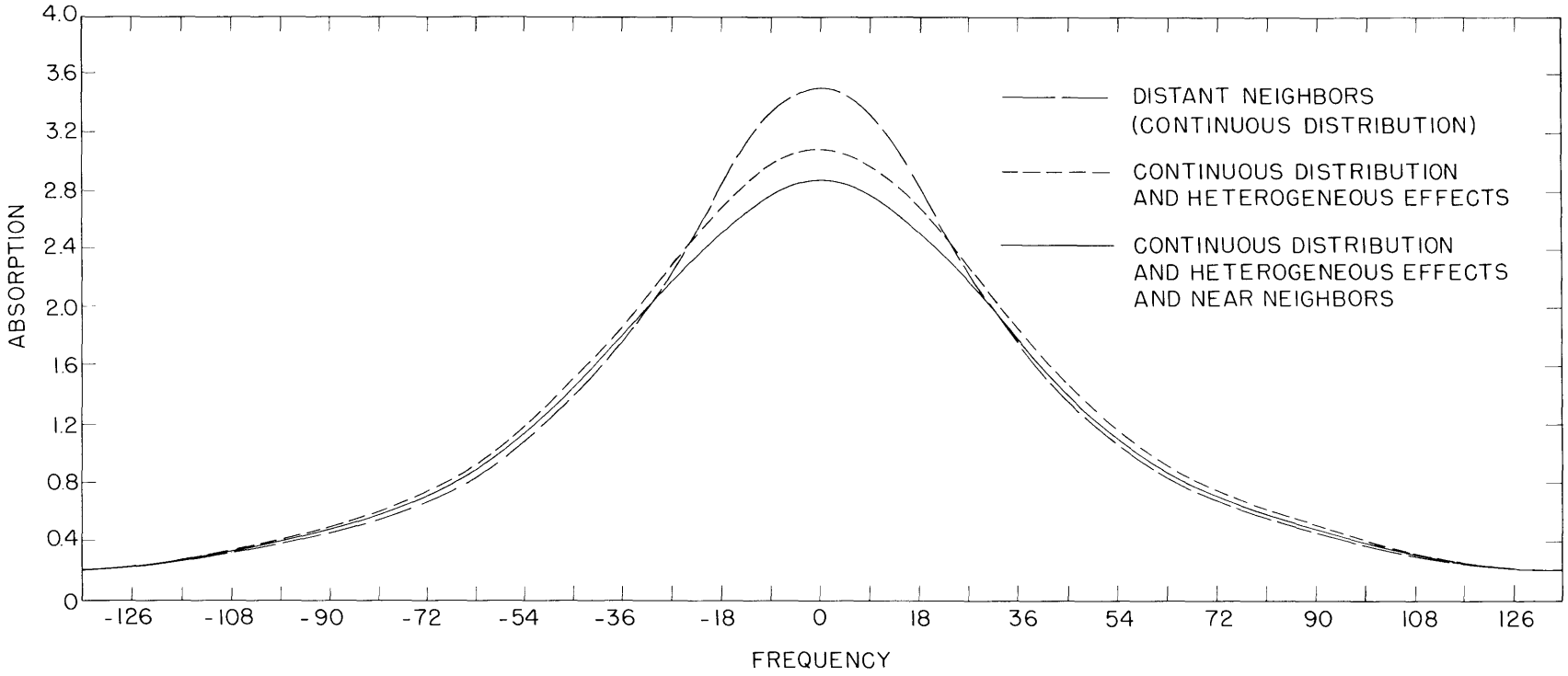

Fig. III-7. Contribution of various effects to the absorption (concentration, 0.2 per cent).

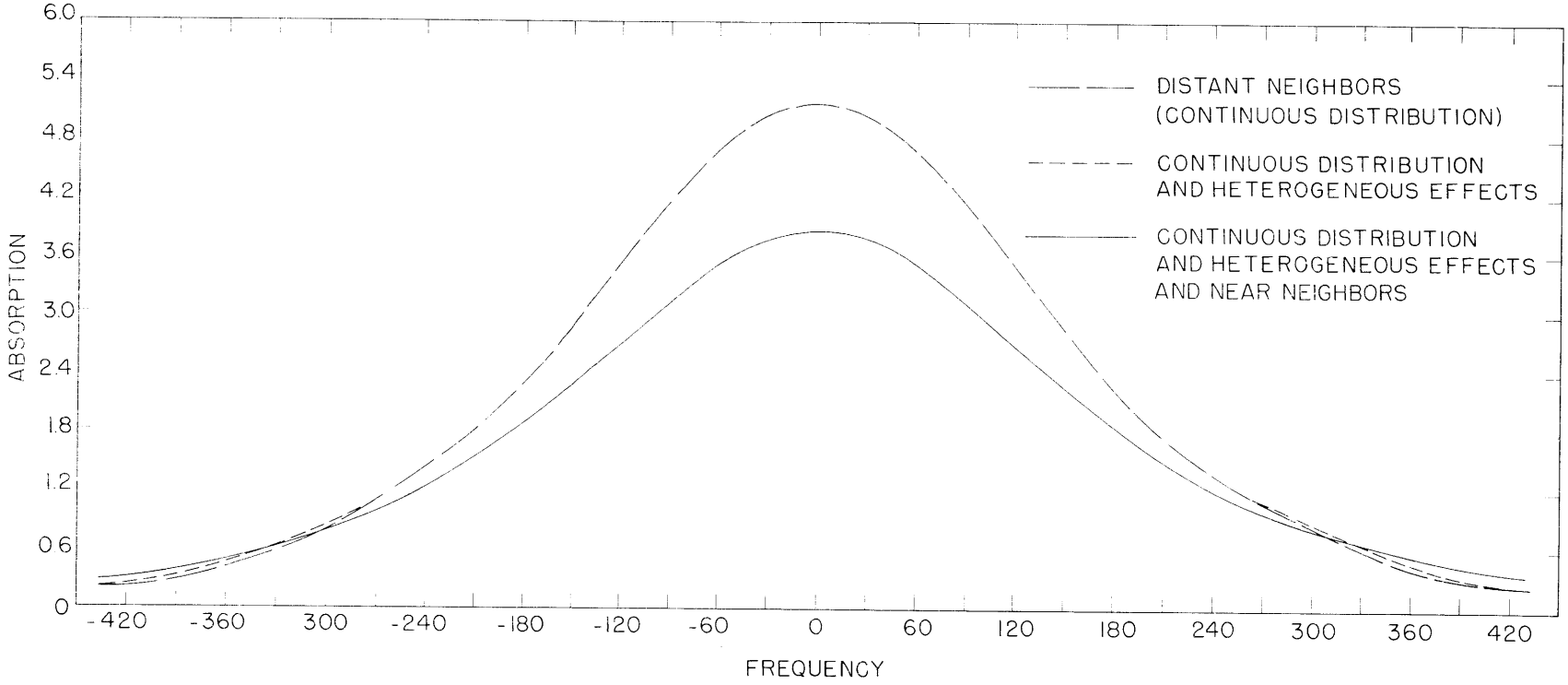

Fig. III-8. Contribution of various effects to the absorption (concentration, 1.1 per cent).

unimportance of the near neighbors in very dilute crystals, although somewhat surprising, can be understood from two considerations: (a) The contribution of these neighbors to the total area varies as n^2. Intuitively, the number of pairs is proportional to n^2; or, more formally, expression (4) shows that the near-neighbor perturbation scales, by a factor n, a line whose area is already proportional to n. (b) While the near neighbors produce the largest single perturbations, the number of neighbors increases faster with distance than the magnitude of their individual perturbations falls off. (It is this same phenomenon that gave rise to the logarithmic divergence that was discussed in the previous report.[1]) As a consequence, for low concentrations, it makes no difference what one assumes about the near neighbors — whether or not they are assumed to be clustered, exchange-coupled, point dipoles, or smeared into a continuous distribution — none of these assumptions will significantly affect the observable part of the line. We note, incidentally, that the reverse is true of the second moment. This quantity weights most heavily the far wings of the line, and it is in the far wings that the near neighbors produce a relatively large effect. If we ignore all of the atoms outside a radius of, say, 7.15 Å, we pick up ~90 per cent of the second moment; if we ignore all of the atoms inside this same radius, we may pick up 90 per cent of the line area.

For concentrations higher than ~0.1 per cent, the near-neighbor contribution to the central part of the line becomes more significant. For the extreme case of very dark ruby, with a concentration of ~1 per cent: (a) The approximation involved in a continuous dipole distribution introduces an error of ~10 per cent when carried as far as the nearest neighbor shell, and an error of 2 or 3 per cent when carried as far as the 10^{th} neighbor shell. (b) The assumption of strong exchange, as opposed to zero exchange, for neighbor shells 10-16 introduces small variations in the calculated widths and intensities, and also tends to make the line slightly more Gaussian. The line derived from

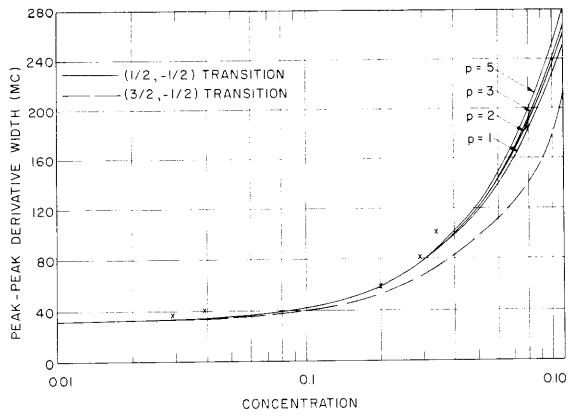

Fig. III-9. Absorption halfwidth vs concentration.

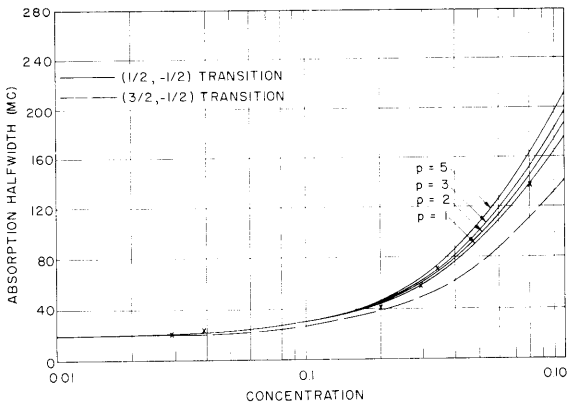

Fig. III-10. Peak absorption vs concentration.

strong exchange agrees slightly better with that derived from the experiment, but the difference is not large enough to be really significant. (c) We can account for the decreased intensity at high concentrations, observed by Manenkov[3] and by us, on the basis of a small amount of clustering. A near-neighbor concentration that is in excess by a factor of 2 or 3 can alter considerably the exponential in (4) and, consequently, the line intensity, although it affects the line shape as a whole only slightly.

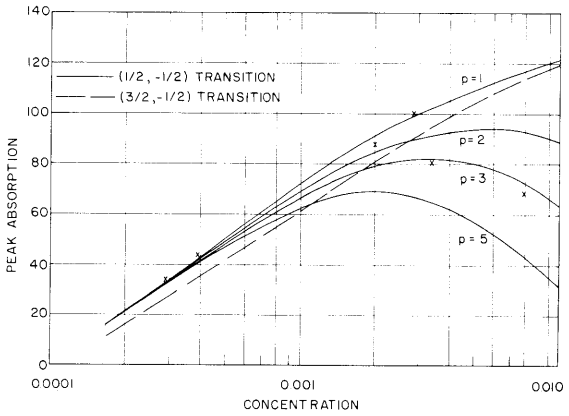

Fig. III-11. Peak-peak derivative width vs concentration.

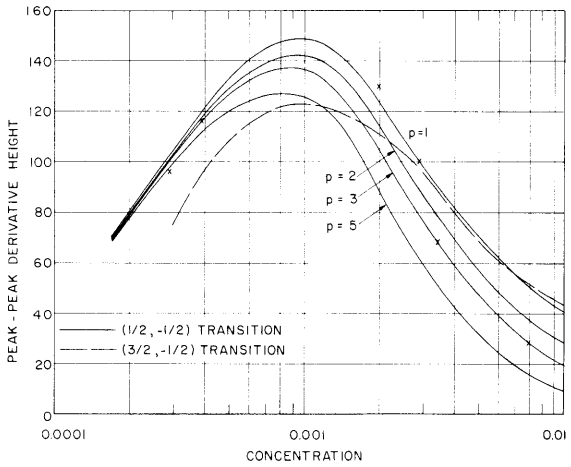

Fig. III-12. Peak-peak derivative height vs concentration.

We exhibit in Figs. III-9, III-10, III-11, and III-12 the calculated behavior of various line-shape parameters. The lines have been calculated with a continuous distribution as far in as the 16^{th}-neighbor shell, and strong exchange is assumed for the near-neighbor shells 1-15. The parameter p is a measure of the assumed clustering and is defined as the ratio of the near-neighbor concentration to the over-all concentration. The scale for intensities has been chosen to match the calculated intensity for 0.3 per cent to the intensity of sample 4. The points shown are experimental and apply to the $\left(\frac{1}{2}, -\frac{1}{2}\right)$ transition.

Figure III-13 shows the calculated variation of the line shape with halfwidth. The line shape goes from Gaussian to Lorentzian as the contribution of Cr-Cr broadening becomes more significant. For extremely broad lines, the Cr-Cr dipolar contribution itself begins to depart somewhat from the Lorentzian. The points shown are experimental.

We now discuss briefly our experimental verification of the calculations. Although data on linewidths and intensities have been published,[3] complete line shapes have not. We used 6 rubies, all grown by the flame-fusion process. Two of these (No. 1 and No. 4) were slow-grown annealed crystals with controlled homogeneity and concentration. We

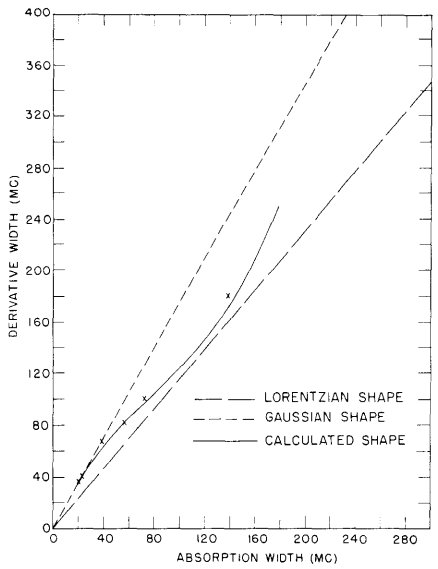

Fig. III-13. Absorption halfwidth vs peak-peak derivative width.

examined polished sections of all of the crystals with a microscope to ensure freedom from macroscopic inhomogeneities. We oriented the boules by the optical method of Mattuck and Strandberg,[4] and had oriented needles cut for use in the spectrometer. Our spectra show a signal-to-noise ratio of at least 100. Accuracy of linewidth measurements is within ~3 per cent. The relative intensities are accurate to ~10 per cent, with crystal No. 4 used as the standard. The experimental derivative curves were integrated to give the absorption, and this, once more, was integrated to give the area.

In Figs. III-14, III-15, and III-16 we give examples of the derivative and absorption curves for samples No. 1, No. 3, and No. 6 (nominal concentrations of 0.03 per cent, 0.2 per cent, 0.8 per cent). To illustrate the progression from Gaussian to Lorentzian shape, we also shown Gaussian and Lorentzian comparison curves, which match the peak value and halfwidth of the experimental absorptions. This progression in shape is predicted by our calculation (see also Fig. III-13).

The data are summarized in Tables III-1 and III-2. Table III-1 contains data that are relevant particularly to concentration measurements. The Cr concentrations were determined by several methods, as indicated in Table III-1. The area of the absorption curve is, of course, also proportional to the concentration. The tabulated areas are also scaled to give the value 0.3 for the $\left(\frac{1}{2},-\frac{1}{2}\right)$ transition of the No. 4 sample. The ratio of the area of the $\left(\frac{3}{2},\frac{1}{2}\right)$ transition to that of the $\left(\frac{1}{2},-\frac{1}{2}\right)$ transition should be 0.75 for all concentrations. This is approximately verified. In Appendix B we explain why we attach little weight to measurements based on integrated absorption areas.

In Table III-2, we call attention to the observed excess width of the $\left(\frac{3}{2},\frac{1}{2}\right)$ transition. The mechanisms included in our calculation predict a narrower, not a broader, line for this transition. We notice: (a) that the excess broadening increases with concentration, and (b) that the annealed crystal No. 4 shows markedly less broadening than the conventionally grown crystals No. 3 and No. 5 of rather similar concentration. Both facts can be explained by ascribing the excess width to random variations of the crystal field parameter D, resulting from internal crystalline strains. Such strains tend to increase with increasing impurity content and are decreased by annealing. Since $\frac{\partial \nu}{\partial \theta} = 0$ at our

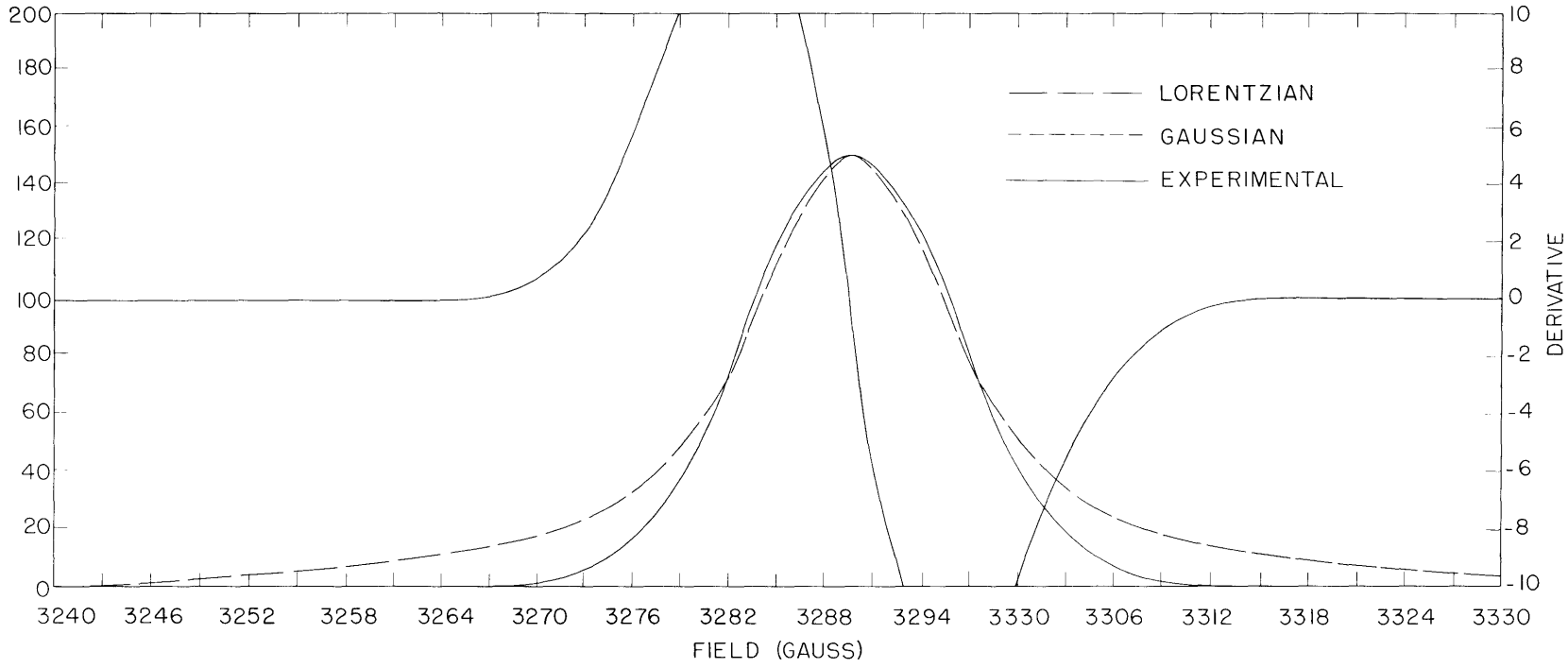

Fig. III-14. Experimental absorption curves and comparison curves (Sample No. 1).

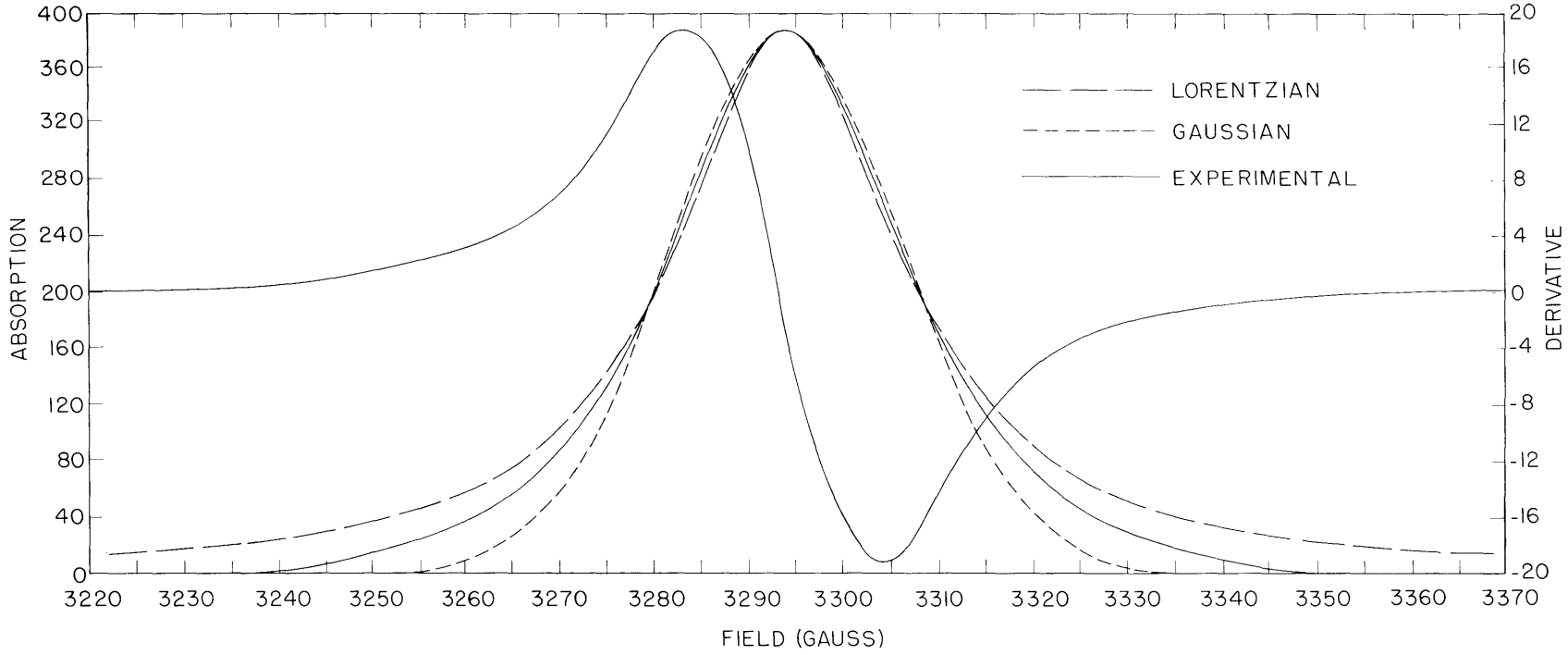

Fig. III-15. Experimental absorption curves and comparison curves (Sample No. 3).

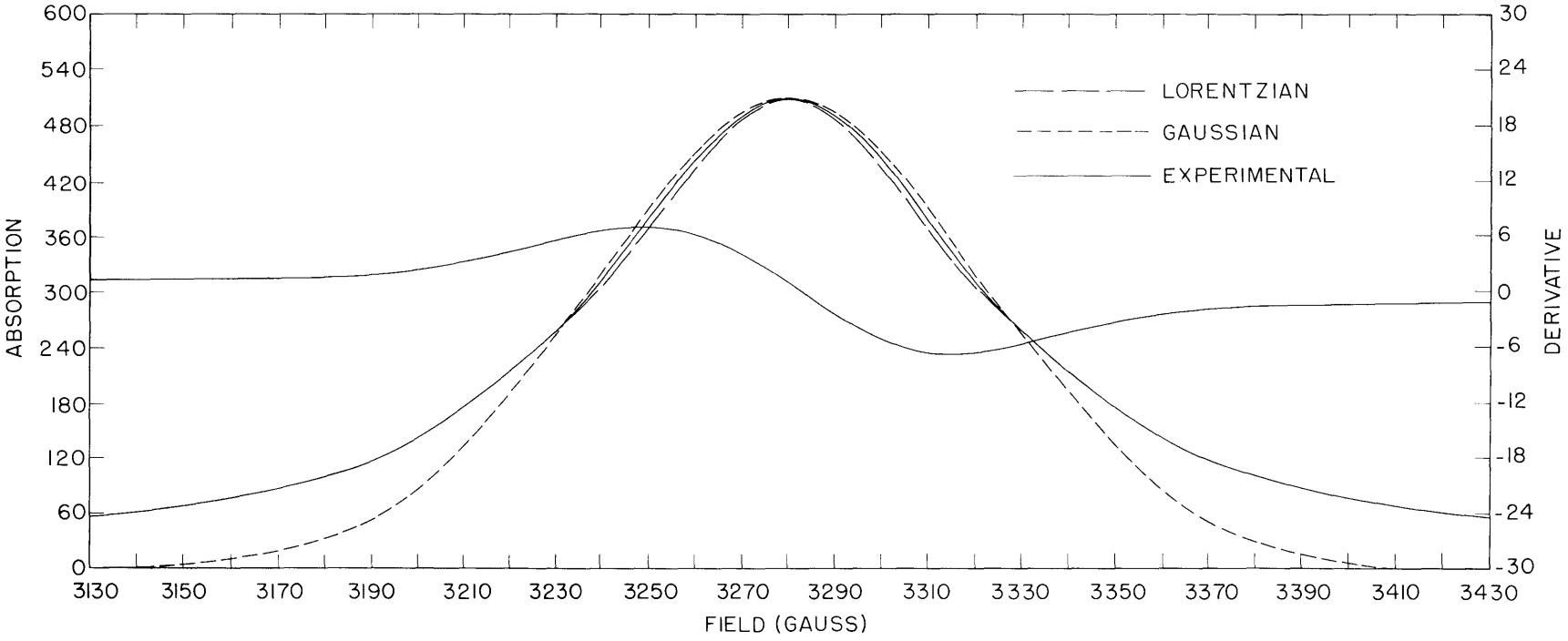

Fig. III-16. Experimental absorption curves and comparison curves (Sample No. 6).

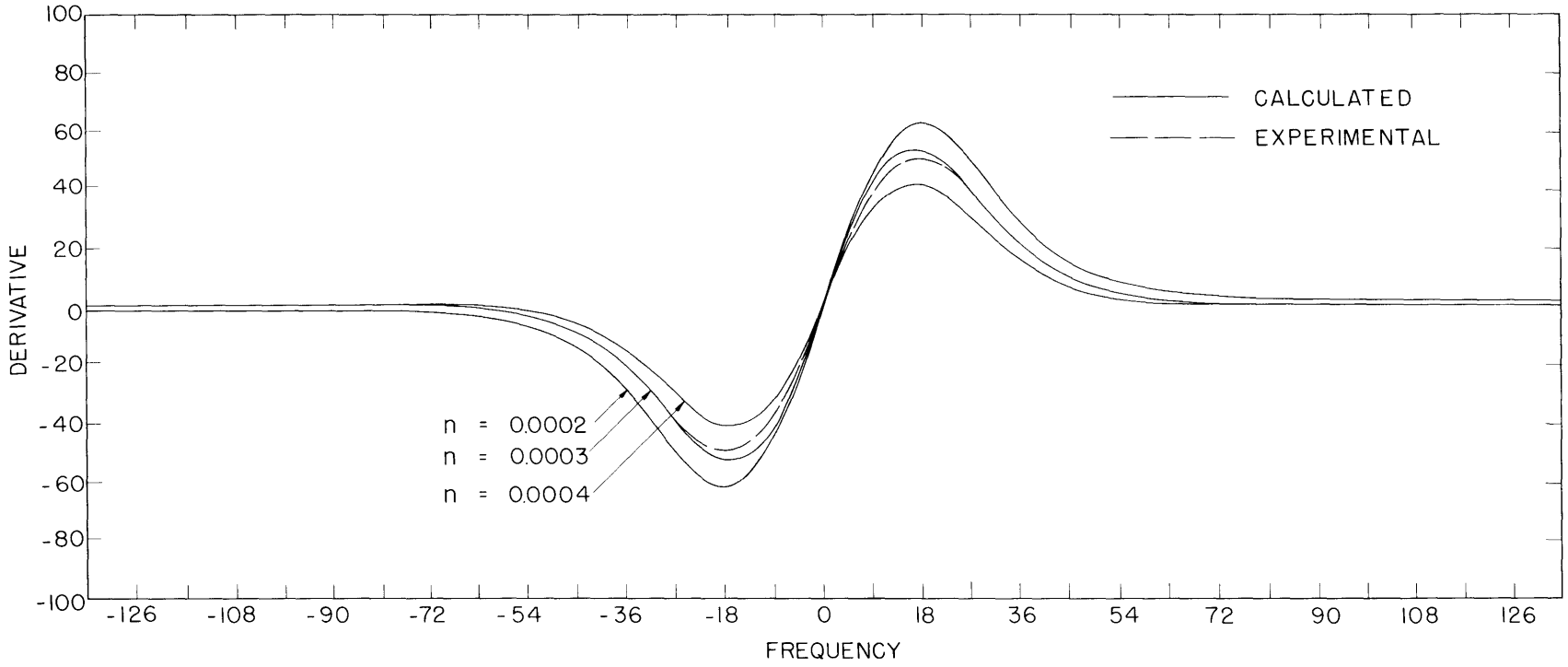

Fig. III-17. Experimental and calculated derivatives (Sample No. 1).

Table III-1. Experimental results.

Sample	Cr Concentration Measurement		Area (1/2, -1/2)	Area (3/2, 1/2)	$\frac{\text{Area}(3/2, 1/2)}{\text{Area}(1/2, -1/2)}$
	Method	Result (per cent)			
1	Process Control	.0336	.036	.026	.72
	Calorimetric	.026			
2	Calorimetric	.039	.05	.031	.63
	Spectrographic	.033			
3	Spectrographic	.20	.19	.12	.63
4	Process Control	.336	.3	.18	.60
	Calorimetric	.28			
5	Calorimetric	.28	.28	.17	.62
	Spectrographic	.34			
6	X-ray	.8	.56	.32	.57
	Calorimetric	.79			

Table III-2. Experimental results.

Sample		1	2	3	4	5	6
$\left(\frac{1}{2}, -\frac{1}{2}\right)$	Derivative P-P Height	96	116	134	100	68	28
	Derivative P-P Width	36.7	39.7	57.3	81.2	100	184
	Absorption Peak	34	44	88	100	81	69
	Absorption Width	21.0	22.9	40.1	58.0	71.0	129
$\left(\frac{3}{2}, \frac{1}{2}\right)$	Derivative P-P Height	54	62	40	44	23	8.1
	Derivative P-P Width	37.6	39.8	85.3	91.3	122.5	283
	Absorption Peak	18	21	34	45	31	25
	Absorption Width	23.4	25.6	57.4	65.8	89.5	203
$\frac{\text{Width}\left(\frac{3}{2}, \frac{1}{2}\right)}{\text{Width}\left(\frac{1}{2}, -\frac{1}{2}\right)}$		1.11	1.12	1.43	1.13	1.27	1.57

0° orientation, small variations in the direction of the crystal field will have no effect; what we appear to see are variations in magnitude.

To illustrate the type of agreement that we obtained between theory and experiment, we present in Figs. III-17, III-18, III-19, and III-20 some experimental curves against a background of theoretical curves clustered around the appropriate concentrations. We stress that, as the concentration increases, the curves do not merely change into magnified reproductions of themselves, but undergo complicated and drastic changes in shape. We bring out this point in Figs. III-21, III-22, III-23, and III-24, in which all of the curves have been scaled to the same peak value. The curves in Figs. III-21 and III-22 are the same, except for scale, as those in Figs. III-19 and III-20. Eliminating any difference in intensity, we see that the shape alone distinguishes concentrations quite sharply. Our calculation predicts not only intensities and halfwidths, but also the detailed variations of the line shape.

The energy eigenvalues for the first seven neighbor shells were obtained by interpolation from the exact diagonalization of the pair Hamiltonians computed by Dr. H. Statz of Raytheon Company, Waltham, Massachusetts. Most of the computations were carried out at the Computation Center, M. I. T.; some were performed at CEIR through the support of the Research Laboratory of Electronics and the National Science Foundation. Miss Gladys McDonald and Miss Ellen McDonald assisted with some of the lengthy and arduous numerical work. Mrs. Barbara T. Grant rendered assistance with programming, numerical calculations, and other numerical aspects of this work.

APPENDIX A

THE RESIDUAL WIDTH

The origin of the residual width of ~18 mc is not obvious. We can rule out spin-lattice processes, which at room temperature can account for ~1 mc.[5] We can rule out the crystal field because the parameter D plays no part in the $\left(\frac{1}{2}, -\frac{1}{2}\right)$ transition.

Magnetic dipole interaction with Al nuclei can be handled by a second-moment calculation. In contrast to Cr-Cr broadening, the concentration of Al nuclei is practically 1. The Gaussian limit should give a fair approximation; at least it gives a valid upper limit for the halfwidth, and this is sufficient for our present purpose. We have done a moment calculation, following the general method of Van Vleck,[6] and have also calculated the relevant crystal sum. In connection with this calculation, we proved, incidentally, that when calculating the Van Vleck moments resulting from the interaction of unlike atoms, the ground-state splitting is irrelevant – that is, the use of projection operators gives the same result that would be given if we had ignored the multiplicity of transitions to start with. We obtain for the halfwidth that is due to dipole interaction with Al nuclei the value 5.12 mc.[7] Since Gaussians add width in rms fashion, this leaves

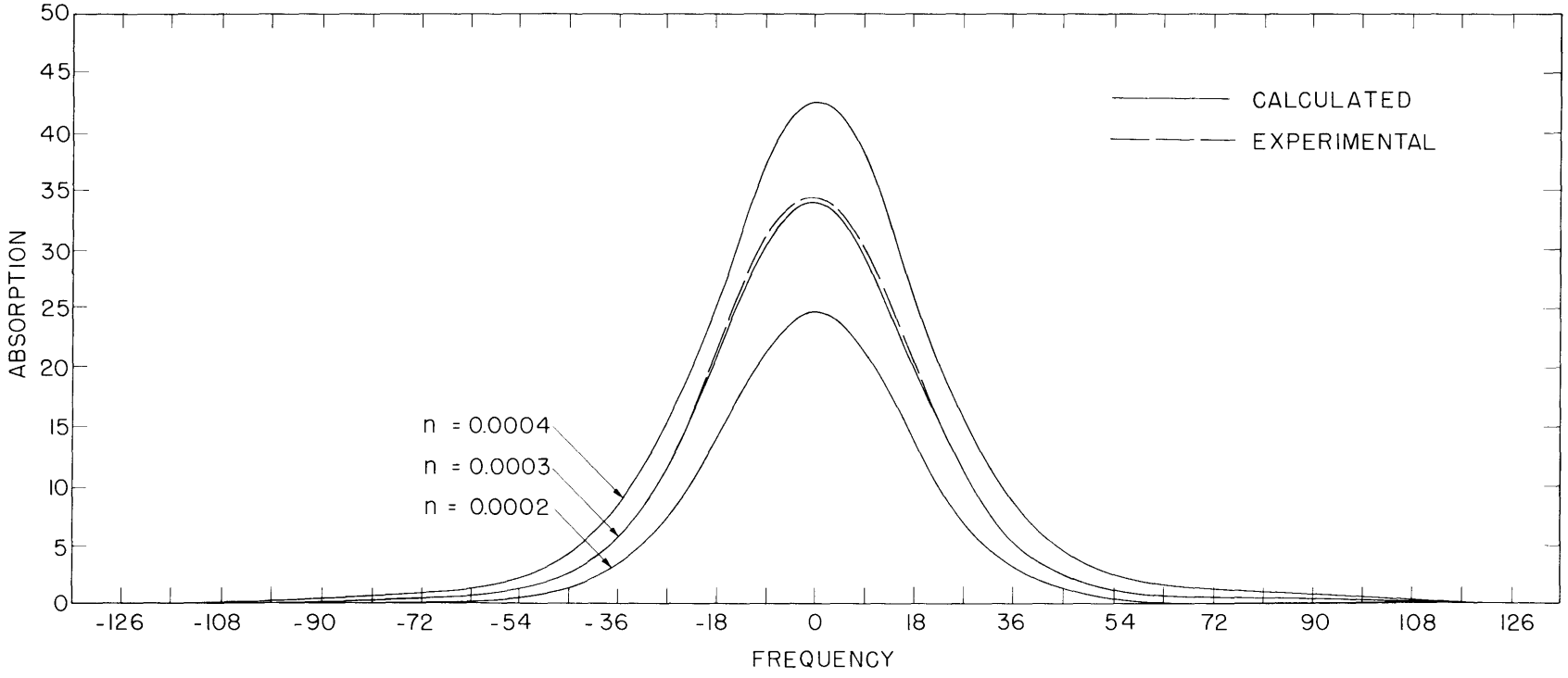

Fig. III-18. Experimental and calculated absorptions (Sample No. 1).

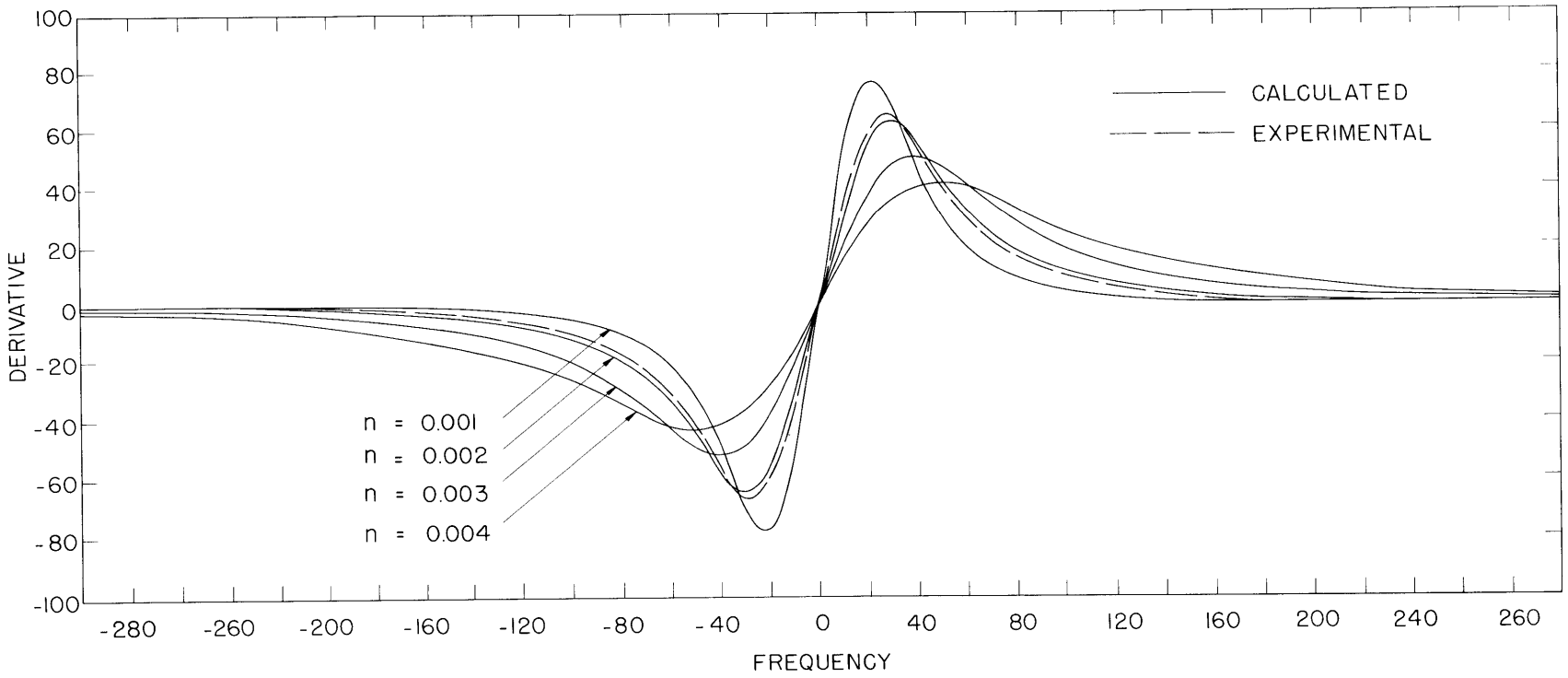

Fig. III-19. Experimental and calculated derivatives (Sample No. 3).

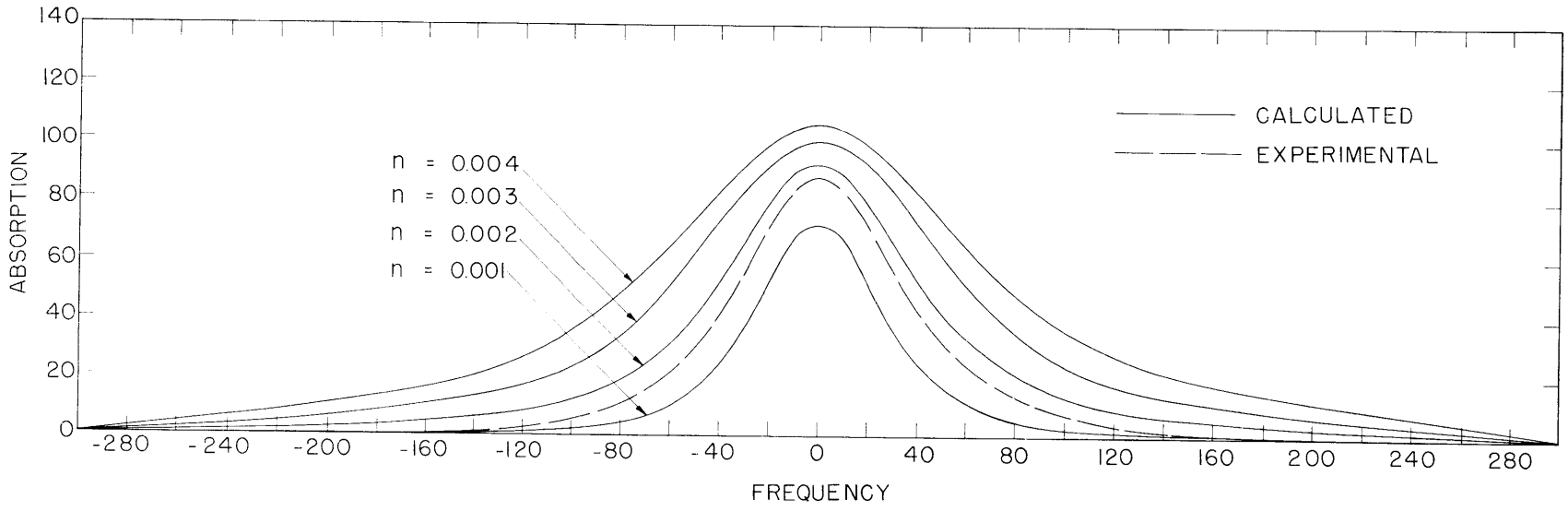

Fig. III-20. Experimental and calculated absorptions (Sample No. 3).

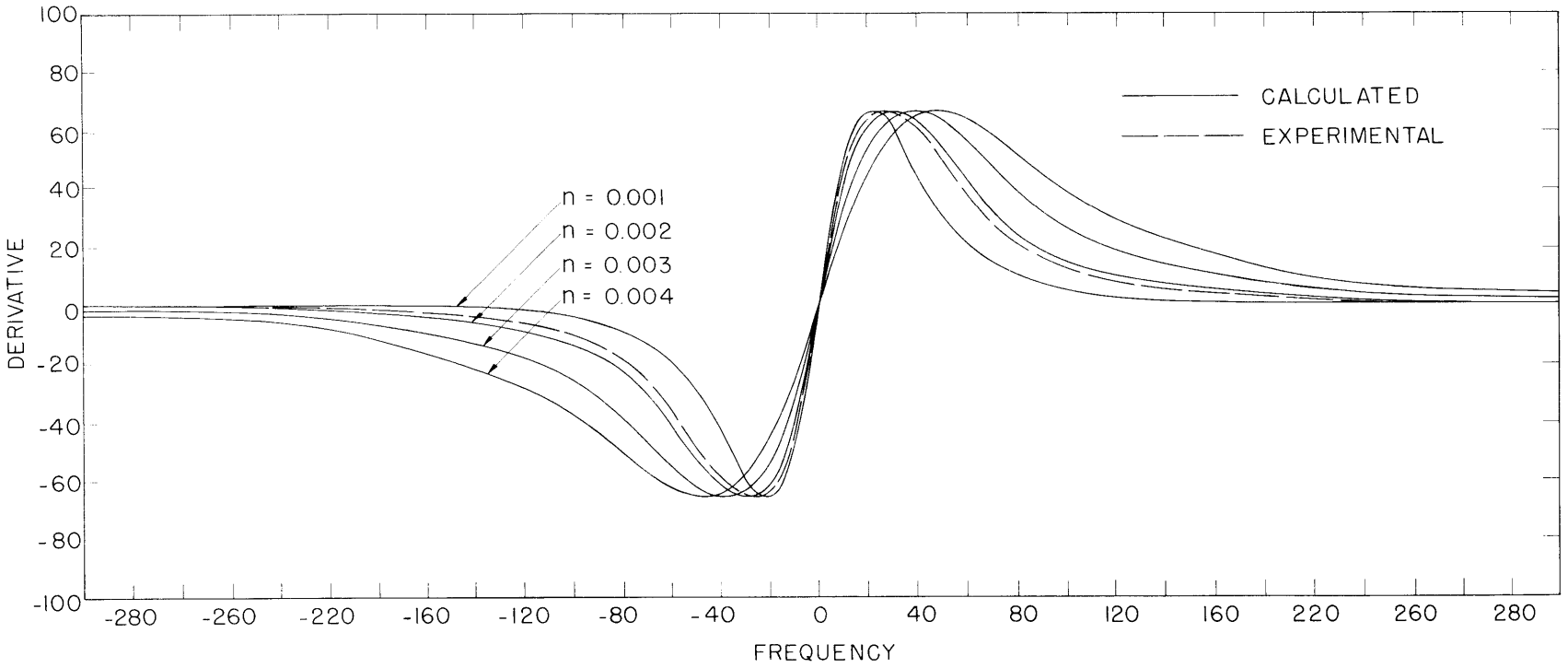

Fig. III-21. Experimental and scaled calculated derivatives (Sample No. 3).

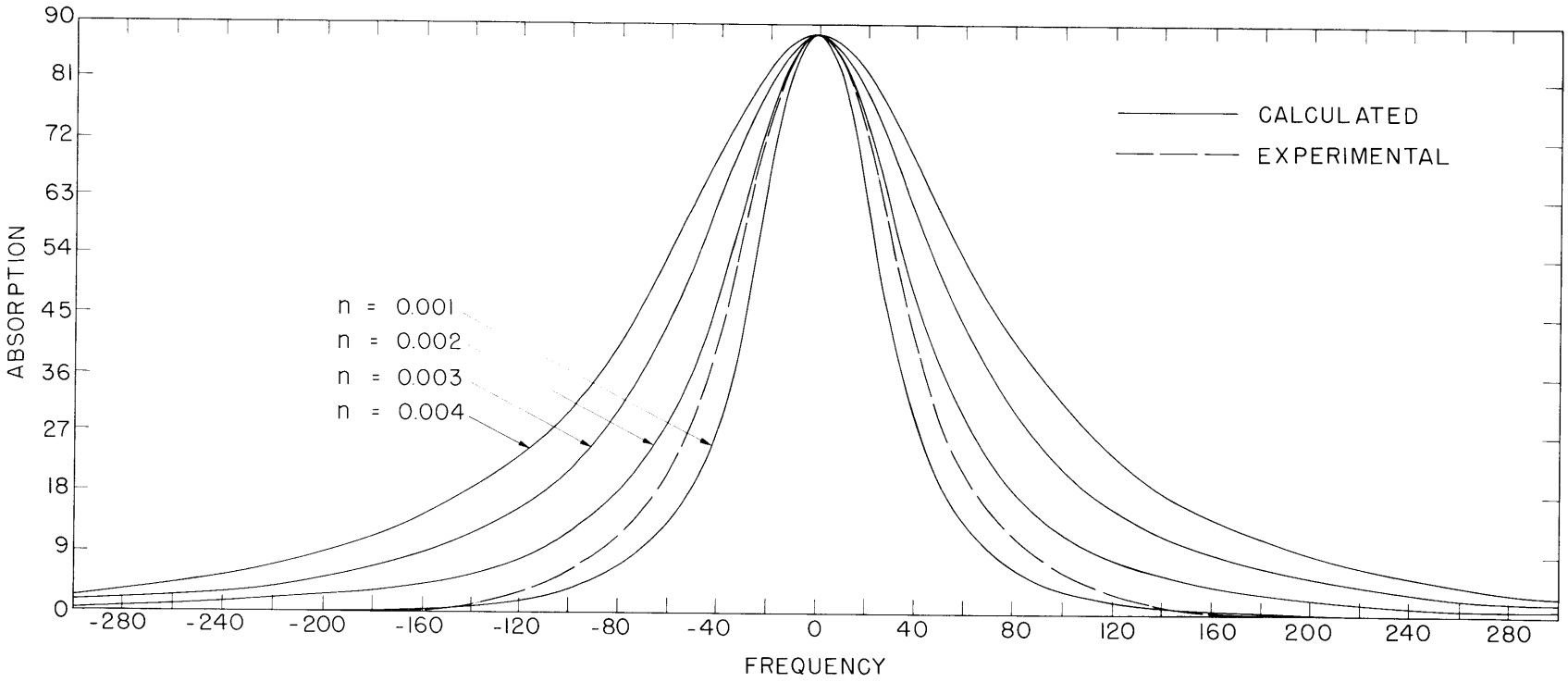

Fig. III-22. Experimental and scaled calculated absorptions (Sample No. 3).

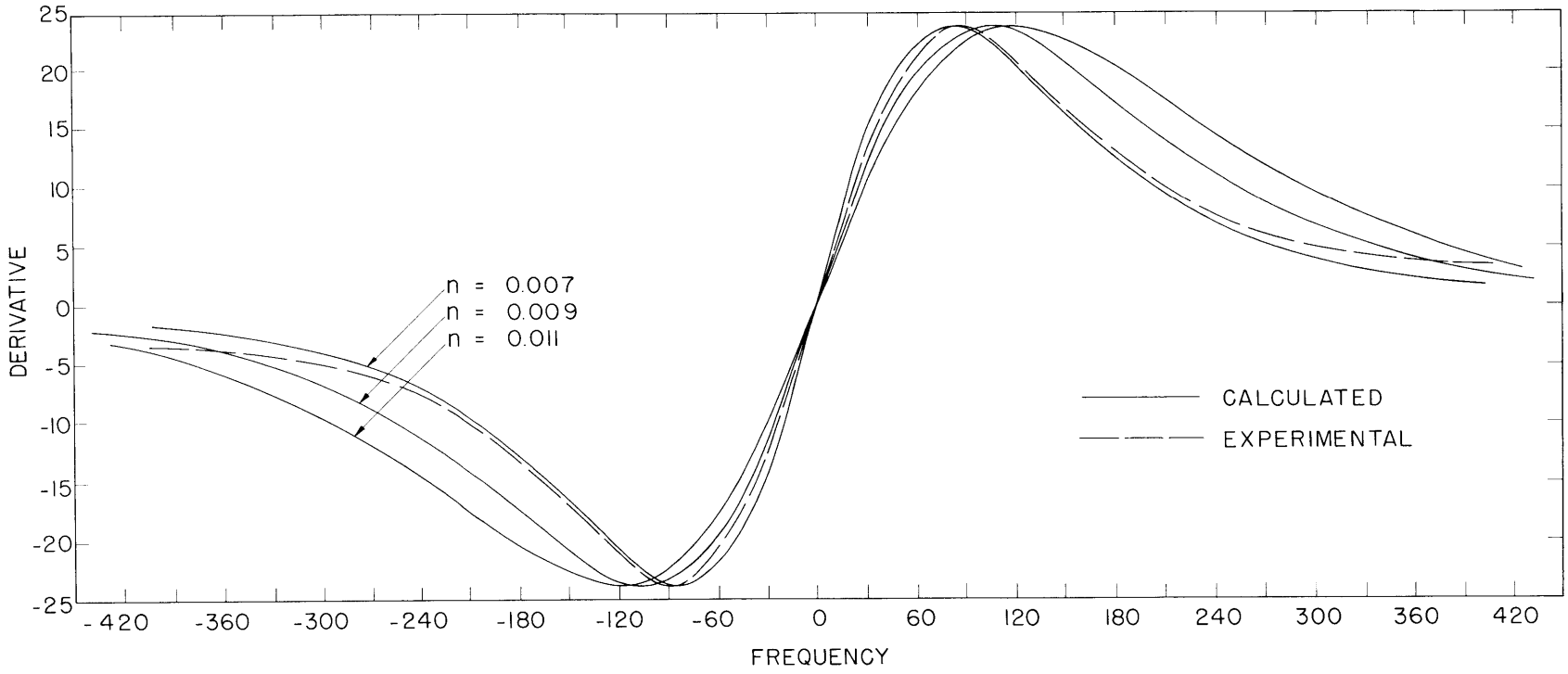

Fig. III-23. Experimental and scaled calculated derivatives (Sample No. 6).

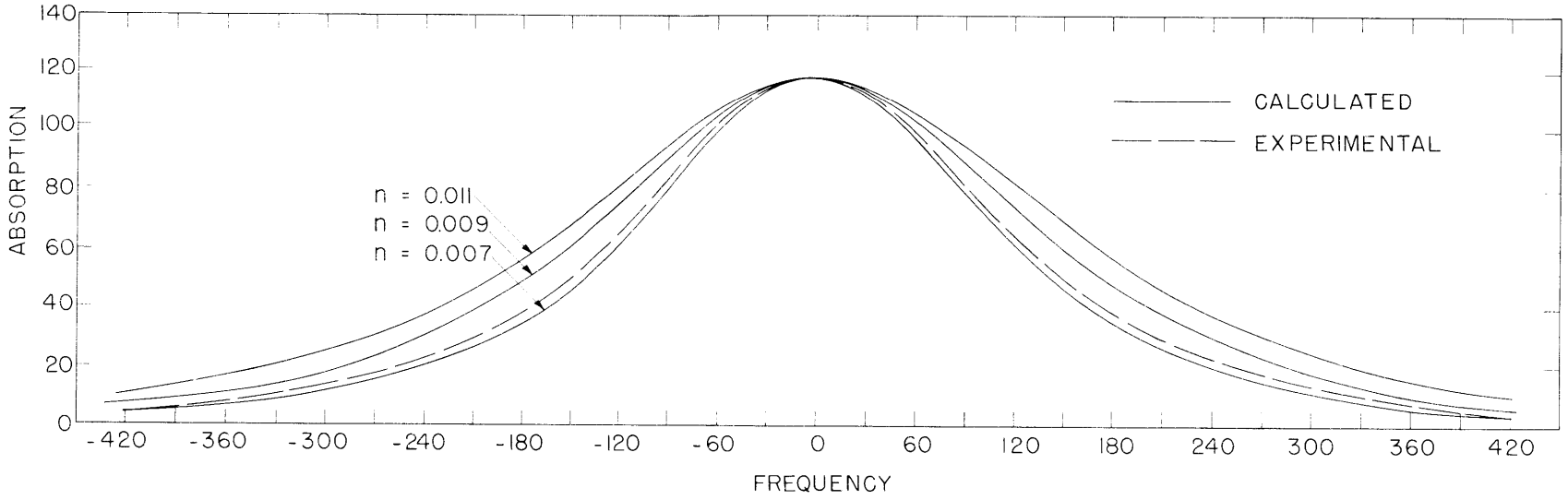

Fig. III-24. Experimental and scaled calculated absorptions (Sample No. 6).

17 mc still unaccounted for.

We feel it is not unreasonable to attribute this residual width to contact interaction of the Cr 3d electrons with the neighboring Al nucleus. If we write the wave function of a Cr 3d electron as $\psi = \psi(\mathrm{Cr}, 3d) + \epsilon\psi(\mathrm{Al}, 3s)$, we can argue, from the measured hyperfine separation in aluminum,[8] that, to account for the observed width, $\epsilon \approx 0.035$. Thus the required amount of covalent bonding does not seem unreasonable. The present suggestion seems attractive because it would also account for the absence of a residual broadening of the Cr spectrum in MgO (Mg has no nuclear moment) and for the fact that the ratio of residual widths of Fe and Cr in Al_2O_3 is approximately the same as the ratio of 3d electrons in these two ions.

APPENDIX B

NOTES ON NUMERICAL COMPUTATIONS

A great deal of effort was spent constructing optimally accurate and efficient programs for our numerical computations. The Fourier inversions were held to an error of 1 part in 10^4 and were carried to ~100 halfwidths. The points were spaced in such fashion that any intermediate point could be obtained to this accuracy with, at most, a 4-point interpolation. Our routine does approximately 10 such transforms in 3 minutes. For the Gaussian convolutions we allowed approximately twice this error in the central part of the line, with a maximum error of ~1 per cent in the extreme wings. The lattice-sum calculation involves the superposition of approximately 40 interpolated curves, and the error cannot be predetermined with such precision; a reasonable estimate is 1 per cent in the central part of the line, and a few per cent in the extreme wings. To facilitate direct comparison of the calculations with experimental data, the final absorptions were differentiated by means of a 3-point Lagrange formula.

In the analysis of experimental data, the experimental traces were digitalized, by using at least six points per halfwidth. The two integrations, to obtain the absorption curve and the area of the absorption, were performed by computer. We investigated the effect of noise and of base-line drift on the results. In general, halfwidths proved quite insensitive, line shapes (Gaussian or Lorentzian) moderately sensitive, and the area extremely sensitive; thus a 2 per cent variation in halfwidth might be associated with a 30 per cent variation in area.

W. J. C. Grant

References

1. W. J. C. Grant, Line shapes of paramagnetic chromium resonance in ruby, Quarterly Progress Report No. 64, Research Laboratory of Electronics, January 15, 1962, pp. 23-34.

2. See, for example, W. Feller, An Introduction to Probability Theory and Its Applications (John Wiley and Sons, Inc., New York, 1957), p. 250 ff.

3. A. A. Manenkov and A. M. Prokhorov, Soviet Phys.-JETP 11, 751 (1960). Our results differ somewhat from their results, although there is a qualitative agreement. One source of discrepancy may lie in the techniques employed to obtain absorption curves from the experimental derivatives. Our method makes no a priori assumptions regarding the line shape, nor is it based on the measurement of one or two parameters. Still another source of discrepancy may lie in the technique used to measure concentrations. We feel that the measurement of absorption areas is the least reliable of available methods, and we have therefore made several other determinations as well.

4. R. D. Mattuck and M. W. P. Strandberg, Rev. Sci. Instr. 30, 195 (1959).

5. A. A. Manenkov and A. M. Prokhorov, op. cit., p. 527.

6. J. H. Van Vleck, Phys. Rev. 74, 1168 (1948).

7. A. A. Manenkov and A. M. Prokhorov, op. cit., p. 751, obtain a halfwidth of 6.25 mc. The discrepancy is not significant for our purpose.

8. H. Lew, Phys. Rev. 76, 1086 (1949).